OPEN

Deep Learning–Enhanced Accelerated 2D TSE and 3D Superresolution Dixon TSE for Rapid Comprehensive Knee Joint Assessment

Céline Smekens, MSc, Quinten Beirinckx, PhD, Frederik Bosmans, MD, Floris Vanhevel, MSc, Annemiek Snoeckx, MD, PhD, Jan Sijbers, PhD, Ben Jeurissen, PhD, Thomas Janssens, PhD, and Pieter Van Dyck, MD, PhD

Objectives: The aim of this study was to evaluate the use of a multicontrast deep learning (DL)–reconstructed 4-fold accelerated 2-dimensional (2D) turbo spin echo (TSE) protocol and the feasibility of 3-dimensional (3D) superresolution reconstruction (SRR) of DL-enhanced 6-fold accelerated 2D Dixon TSE magnetic resonance imaging (MRI) for comprehensive knee joint assessment, by comparing image quality and diagnostic performance with a conventional 2-fold accelerated 2D TSE knee MRI protocol.

Materials and Methods: This prospective, ethics-approved study included 19 symptomatic adult subjects who underwent knee MRI on a clinical 3 T scanner. Every subject was scanned with 3 DL-enhanced acquisition protocols in a single session: a clinical standard 2-fold in-plane parallel imaging (PI) accelerated 2D TSE-based protocol (5 sequences, 11 minutes 23 seconds) that served as a reference, a DL-reconstructed 4-fold accelerated 2D TSE protocol combining 2-fold PI and 2-fold simultaneous multislice acceleration (5 sequences, 6 minutes 24 seconds), and a 3D SRR protocol based on DL-enhanced 6-fold accelerated (ie, 3-fold PI and 2-fold simultaneous multislice) 2D Dixon TSE MRI (6 anisotropic 2D Dixon TSE acquisitions rotated around the phase-encoding axis, 6 minutes 24 seconds). This resulted in a total of 228 knee MRI scans comprising 21,204 images. Three readers evaluated all pseudonymized and randomized images in terms of image quality using a 5-point Likert scale. Two of the readers (musculoskeletal radiologists) additionally evaluated anatomical visibility and diagnostic confidence to assess normal and pathological knee structures with a 5-point Likert scale. They recorded the presence and location of internal knee derangements, including cartilage defects, meniscal tears, tears of ligaments, tendons and muscles, and bone injuries. The statistical analysis included nonparametric Friedman tests, and interreader and intrareader agreement assessment using the weighted Fleiss-Cohen kappa (κ) statistic. *P* values of less than 0.05 were considered statistically significant.

Results: The evaluated DL-enhanced 4-fold accelerated 2D TSE protocol provided very similar image quality and anatomical visibility to the standard 2D TSE protocol, whereas the 3D SRR Dixon TSE protocol scored less in terms of overall image quality due to reduced edge sharpness and the presence of artifacts ($P < 0.001$). Subjective signal-to-noise ratio, contrast resolution, fluid brightness, and fat suppression were good to excellent for all protocols. For 1 reader, the Dixon method of the 3D SRR protocol provided significantly better fat suppression than the spectral fat saturation applied in the standard 2D TSE protocol ($P < 0.05$). The visualization of knee structures with 3D SRR Dixon TSE was very similar to the standard protocol, except for cartilage, tendons, and bone, which were affected by the presence of reconstruction and aliasing artifacts ($P < 0.001$). The diagnostic confidence of both readers was high for all protocols and all knee structures, except for cartilage and tendons. The standard 2D TSE protocol showed a significantly higher diagnostic confidence for assessing tendons than 3D SRR Dixon TSE MRI ($P < 0.01$). The interreader and intrareader agreement for the assessment of internal knee derangements using any of the 3 protocols was substantial to almost perfect ($\kappa = 0.67–1.00$). For cartilage, the interreader agreement was substantial for DL-enhanced accelerated 2D TSE ($\kappa = 0.79$) and almost perfect for standard 2D TSE ($\kappa = 0.98$) and 3D SRR Dixon TSE ($\kappa = 0.87$). For menisci, the interreader agreement was substantial for 3D SRR Dixon TSE ($\kappa = 0.70–0.80$) and substantial to almost perfect for standard 2D TSE ($\kappa = 0.80–0.99$) and DL-enhanced 2D TSE ($\kappa = 0.87–1.00$). Moreover, the total acquisition time was reduced by 44% when using the DL-enhanced accelerated 2D TSE or 3D SRR Dixon TSE protocol instead of the conventional 2D TSE protocol.

Conclusions: The presented DL-enhanced 4-fold accelerated 2D TSE protocol provides image quality and diagnostic performance similar to the standard 2D protocol. Moreover, the 3D SRR of DL-enhanced 6-fold accelerated 2D Dixon TSE MRI is feasible for multicontrast 3D knee MRI as its diagnostic performance is comparable to standard 2-fold accelerated 2D knee MRI. However, reconstruction and aliasing artifacts need to be further addressed to guarantee a more reliable visualization and assessment of cartilage, tendons, and bone. Both the 2D and 3D SRR DL-enhanced protocols enable a 44% faster examination compared with conventional 2-fold accelerated routine 2D TSE knee MRI and thus open new paths for more efficient clinical 2D and 3D knee MRI.

Key Words: deep learning, diagnostic knee MRI, 2-dimensional, 3-dimensional, parallel imaging, simultaneous multislice, turbo spin echo, Dixon, superresolution reconstruction

(*Invest Radiol* 2025;60: 220–233)

To this day, multicontrast 2-dimensional (2D) turbo spin echo (TSE) magnetic resonance imaging (MRI) remains the backbone of clinical knee MRI due to its excellent tissue contrast.[1,2] Standard-of-care 2D TSE protocols typically consist of fluid-sensitive proton density (PD)–weighted, intermediate-weighted (IW), and T2-weighted sequences with or without fat suppression (FS), as well as a fat-sensitive T1-weighted sequence.[3,4] Although these sequences yield high in-plane resolution,

Received for publication May 23, 2024; and accepted for publication, after revision, July 9, 2024.

From the imec-Vision Lab, Department of Physics, University of Antwerp, Antwerp, Belgium (C.S., Q.B., J.S., B.J.); Siemens Healthcare NV/SA, Groot-Bijgaarden, Belgium (C.S., T.J.); Department of Radiology, Antwerp University Hospital, Antwerp, Belgium (F.B., F.V., A.S., P.V.D.); and MIRA, Faculty of Medicine and Health Sciences, University of Antwerp, Antwerp, Belgium (A.S., P.V.D.).

Conflicts of interest and sources of funding: This work was supported by the B-Q MINDED project, funded by European Union's Horizon 2020 research and innovation program under the Marie Sklodowska-Curie grant agreement no. 764513. C.S. and Q.B. also received funding from the University of Antwerp (BOF/SEP #44883 and IOF/SBO #34427, respectively). P.V.D. and B.J. are supported by the Research Foundation (FWO) Flanders, Belgium (grant number G058723N). T.J. and C.S. are employees of Siemens Healthcare NV/SA. The funders and employers had no role in the design, implementation, or analysis of this research. For the remaining authors, none were declared.

Correspondence to: Céline Smekens, MSc, imec-Vision Lab, Department of Physics, University of Antwerp, Universiteitsplein 1, Building N, B-2610 Antwerp, Belgium. E-mail: celine.smekens@uantwerpen.be.

ISSN: 0020-9996/25/6003–0220
DOI: 10.1097/RLI.0000000000001118

their considerable voxel anisotropy (relatively larger slice thickness) comes with disadvantages such as partial volume effects and an increased total scan time due to separate multiplanar acquisitions.[5]

To speed up the 2D TSE acquisitions, advanced acceleration techniques such as parallel imaging (PI), simultaneous multislice (SMS) acquisition, and compressed sensing (CS) have been successfully adopted into the clinic, and their synergies have been exploited.[1,6–8] When using only PI, the acceleration factor is typically limited to 2 or 3 (depending on the coil characteristics) due to the corresponding loss in signal-to-noise ratio (SNR).[2] However, the combined use of PI and SMS enables clinical 4-fold accelerated acquisitions with preservation of image quality and diagnostic performance, leading to comprehensive knee MRI examinations that are approximately 50% faster than the conventional PI-only 2-fold accelerated 2D TSE knee protocols.[8,9]

Recently, advanced deep learning (DL) image reconstruction methods based on supervised learning techniques with convolutional neural networks have been introduced for accelerated 2D TSE MRI by all major MRI vendors.[10–12] In contrast to conventional image reconstruction methods, these new DL techniques break with the traditional MRI trade-off among SNR, spatial resolution, and acquisition time and are thus able to simultaneously enhance the image quality and reduce the acquisition time.[13] Two recent studies investigating the use of DL image reconstruction for 2-fold PI accelerated 2D TSE knee MRI reported a total scan time reduction of approximately 50%, either by halving the number of averages or doubling the acceleration factor (resulting in a 4-fold PI acceleration).[14,15] They also recorded better image quality and preserved diagnostic confidence compared with the standard 2D TSE protocols. Similar results were obtained in a study investigating the use of CS together with a DL-based in-plane superresolution reconstruction (SRR) approach for 2D knee MRI.[16] Another study looked into DL image reconstruction of 4-fold accelerated 2D TSE knee MRI combining PI and SMS and found higher SNR and better spatial resolution compared with conventionally reconstructed 4-fold accelerated 2D TSE acquisitions.[13] Moreover, Kim et al[17] found the use of higher acceleration factors (up to 8-fold) with DL image reconstruction to be clinically feasible for sagittal 2D TSE with fat-saturated T2-weighted contrast and claimed this to be applicable to other contrasts and orientations. The latter may however require the development of specifically trained and tailored convolutional neural networks.[13] Overall, DL-reconstructed highly accelerated comprehensive 2D TSE knee MRI protocols still require further clinical validation to achieve a secure and widespread implementation in clinical practice.

A viable alternative for 2D TSE knee MRI is 3-dimensional (3D) TSE imaging, which has undergone a great evolution over the past decade. 3D TSE sequences, such as 3D sampling perfection with application optimized contrast using different flip angle evolutions (SPACE) TSE, have benefited from advanced acceleration techniques such as PI, 2D controlled aliasing in PI results in higher acceleration (CAIPIRINHA), and CS to provide single-contrast high-resolution isotropic 3D TSE images with diagnostic image quality in a less than 5 minutes.[18–21] Consequently, it has become possible to perform comprehensive 3D knee MR examinations within 10 minutes time. Despite the inherent advantages of 3D TSE knee MRI, such as decreased partial volume effects and multiplanar reformatting, and their demonstrated interchangeability with standard 2D TSE protocols, 3D TSE MRI has not yet replaced the current clinical standard protocols as radiologists seem to prefer the image quality and more familiar contrasts obtained with 2D TSE sequences.[5,22,23]

An alternative way of obtaining 3D TSE MRI while preserving 2D TSE contrasts is through 3D SRR of 2D TSE MRI.[24–26] Previously, an SRR method based on rotated 2D acquisitions with low through-plane resolution was found to be technically feasible for high-resolution isotropic knee MRI.[26] However, the relatively long acquisition time of the presented single-contrast 3D SRR protocol hindered its clinical validation.

By further accelerating the 2D input data acquisition and incorporating a multicontrast technique such as the Dixon method,[27] the acquisition time of a 3D SRR TSE knee protocol can be greatly reduced. Consequently, we hypothesized that 3D SRR of DL-reconstructed highly accelerated 2D Dixon TSE MRI can generate multicontrast images with sufficient image quality for comprehensive knee joint evaluation in a competitive acquisition time compared with a state-of-the-art DL-enhanced accelerated 2D TSE protocol. Therefore, the aim of this study was 2-fold: (1) to add to the evidence that a comprehensive protocol consisting of DL-enhanced accelerated 2D TSE sequences is a suitable option for rapid 2D knee MRI; and (2) to evaluate the feasibility of a time-competitive 3D SRR DL-enhanced 2D Dixon TSE MRI protocol for comprehensive knee joint assessment through comparison to conventional 2D TSE knee MRI.

Materials and Methods

Study Design

This prospective, single-center study was approved by our institutional ethics committee (registration number B300201627688) and was conducted according to the principles of the 1964 Declaration of Helsinki and its later amendments.

The study included 19 adult patients with clinical indications for knee MRI and without general contraindications for MRI. Patients who previously underwent arthroscopic knee surgery (ie, partial meniscectomy) were not excluded from the study. All participants were recruited between February 2023 and March 2023 and provided written informed consent for study inclusion and prospective data collection. An overview of the patients' demographics and their clinical characteristics is provided in Table 1.

First, a preliminary study was conducted including data collected from 3 participants to familiarize the radiologists with all research protocols and refine the evaluation criteria. Subsequently, 16 participants were included in the main study (6 men, 10 women; mean age ± standard deviation [SD], 40.2 ± 12.7 years; age range, 18–57 years; mean body mass index ± SD, 27.2 ± 4.5 kg/m^2; body mass index range, 20.3–34.4 kg/m^2; right knee, n = 6). All patients, in both the preliminary and main studies, were scanned with the same MRI protocols: a clinical 2D protocol, which served as a standard-of-reference, and 2D and 3D research protocols. This resulted in a total of 228 knee MRI scans comprising 21,204 acquired images. The full MR knee examination of each

TABLE 1. Patient Demographics and Clinical Characteristics

Characteristic	Value
Sex, n	
Female	11
Male	8
Age, y, mean ± SD (range)	
All	40 ± 13 (18–57)
Female	41 ± 14 (18–57)
Male	37 ± 12 (18–56)
Laterality, n	
Left	13
Right	6
Indication for MRI, n	
Acute trauma	6
Chronic pain	11
Postoperative	2

n, number; SD, standard deviation; MRI, magnetic resonance imaging.

patient, including the clinical and research protocols, was carried out in a single scan session. Three readers evaluated all pseudonymized and randomized images twice. The outcome variables were qualitative observations of image quality, visibility of anatomical structures, and diagnostic confidence to assess normal and abnormal knee structures. The findings from the preliminary study were not considered for the statistical analysis of the main study.

A flow diagram illustrating the study design is shown in Figure 1.

MRI Acquisition Protocols

MRI examinations were performed on a commercially available, clinical whole-body 3 T MRI scanner (MAGNETOM Vida XT with a maximum gradient amplitude of 60 mT/m and a maximum slew rate of 200 T/m/s, software version XA31A; Siemens Healthineers, Erlangen, Germany) with an 18-channel transmit/receive knee coil.

All subjects were imaged with a clinical standard 2D TSE-based protocol, including axial and coronal IW FS, coronal T1-weighted, and sagittal PD-weighted and T2-weighted FS acquisitions with a total acquisition time of 11 minutes 23 seconds. This clinical protocol incorporated 2-fold in-plane PI acceleration (ie, PAT 2) combined with the commercially released Deep Resolve techniques Gain and Sharp, that is, a denoising method based on iterative localized denoising using noise maps and a DL-based in-plane SRR technique, respectively.[28–31] Representative images are shown in Figure 2.

In addition to the clinical protocol, subjects were scanned with a research software package from Siemens Healthineers (reference ID: 1062_iTSE), hereafter referred to as "WIP" sequence, enabling DL-reconstructed 4-fold accelerated 2D TSE imaging (ie, PAT 2 × SMS 2 with DL-based denoising and a DL-based in-plane SRR, together further denoted as DL-enhanced) for all required contrasts and orientations in a scan time of 6 minutes 24 seconds.[8,10,17]

For the accelerated 3D SRR research protocol, the Dixon functionality of the WIP sequence was enabled to generate multiple contrasts with a single acquisition. From the 2 acquired contrasts (ie, in-phase and out-of-phase) and 2 in-line reconstructed contrasts (ie, water-only and fat-only), in-phase and water-only images were retained for subsequent through-plane SRR, as shown in Figure 3, to allow for a direct comparison with the clinical 2D contrasts. SRR in the through-plane dimension was performed using 6 rotated DL-enhanced accelerated 2D IW Dixon TSE acquisitions (each acquired with PAT 3 × SMS 2, DL-based denoising and DL-based in-plane SRR), resulting in a total scan time of 6 minutes 24 seconds that matched the 2D research protocol duration. Subsequent repetitions only differed by rotational increments of 30 degrees (ie, 180°/N degrees, with N = 6, the number of rotated acquisitions) around the phase encoding axis. A previously published SRR method using total variation regularization and joint rigid interscan motion estimation/correction[26,32] was used to reconstruct the in-phase and water-only images with a voxel size of $0.35 \times 0.35 \times 2$ mm^3 to an isotropic voxel grid of $0.35 \times 0.35 \times 0.35$ m^3 as illustrated in Figure 3.

The main imaging parameters of the clinical and research protocols are listed in Table 2. The 3 protocols were applied in varying order across all participants to reduce negative bias due to risk of motion.

Image Evaluation

All MRI data from each patient were pseudonymized and separated into 3 individual examinations. The randomly organized 2D and 3D SRR examinations from all patients (ie, total of 48 datasets in the main study) were independently evaluated by 2 musculoskeletal (MSK) radiologists with 21 years (P.V.D., reader A) and 2 years (F.B., reader B) of experience in MSK imaging. Blinded to the subjects' clinical information, they assessed all data in terms of image quality, anatomic visibility, and diagnostic confidence. Additionally, a biomedical engineer with 5 years of experience in MSK MRI (C.S., reader C) independently evaluated the image quality. Every reader performed the evaluation twice with a minimum of 4 weeks between repeated readings. Readings were performed on PACS monitors with 5-megapixel resolution (Barco, Kortrijk, Belgium) in a standardized fashion. Readers were allowed to use their preferred window and level settings, as well as magnification and multiplanar reconstruction mode where preferred.

Image quality variables and the visibility of specific anatomical structures were graded using a 5-point Likert scale[14] (1 = nondiagnostic/complete obscuration of anatomy; 2 = poor quality/severe artifacts present that interfere with the relevant clinical question; 3 = adequate quality/some artifacts present that may interfere with the relevant clinical question; 4 = good quality/minimal artifacts present that do not interfere with the relevant clinical question; 5 = excellent quality/no

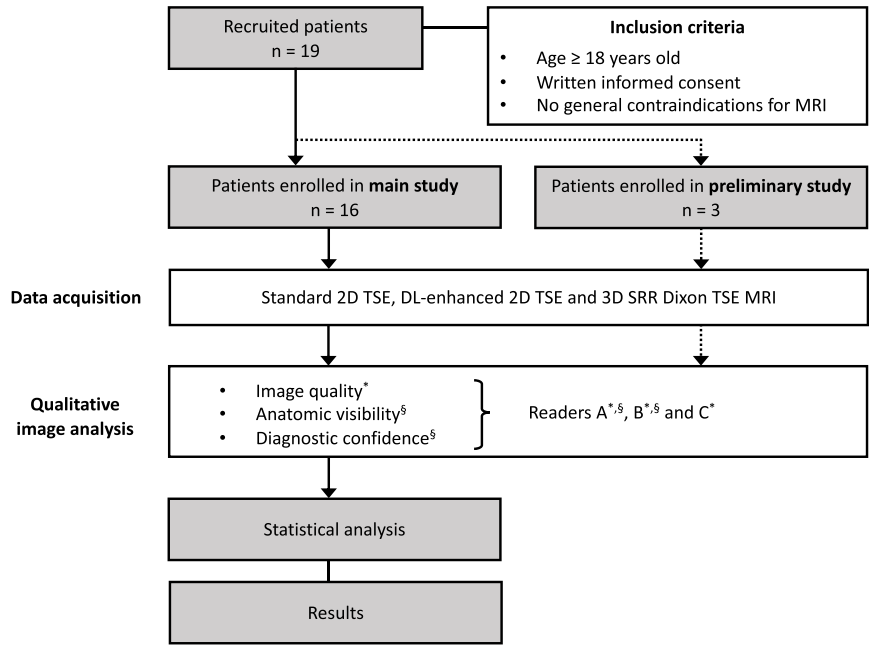

FIGURE 1. Flow diagram of the study design.

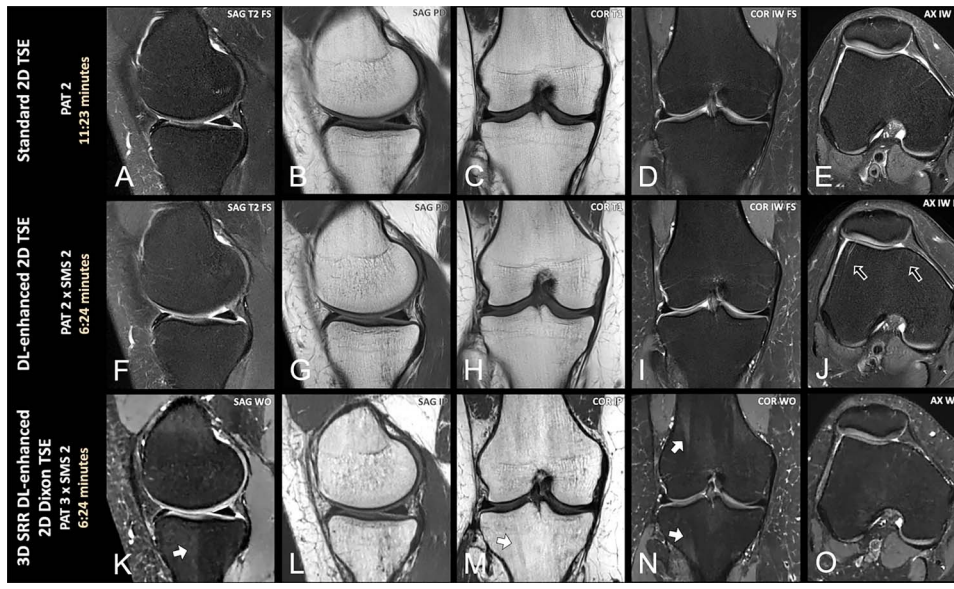

FIGURE 2. Overview of the clinical and research protocols, illustrated for a right knee of a 25-year-old female patient volunteer with sustained knee pain. No lesions were detected on MRI. The MRI protocols for comprehensive knee examination used in this study were: standard 2D TSE (PAT 2, A–E), DL-enhanced 2D TSE (PAT 2 × SMS 2, F–J), and a 3D SRR protocol based on DL-enhanced 2D Dixon TSE data (PAT 3 × SMS 2, K–O). Motion artifacts can be observed in J (black arrows), whereas SRR images (eg, K, M, and N) show aliasing artifacts (white arrows) in the phase-encoding (ie, head to feet) direction, which in turn did not hamper the clinical decision making. SAG, sagittal; COR, coronal; AX, axial; PD, proton density–weighted; IW, intermediate-weighted; T1, T1-weighted; T2, T2-weighted; FS, fat suppressed; WO, water-only; IP, in-phase.

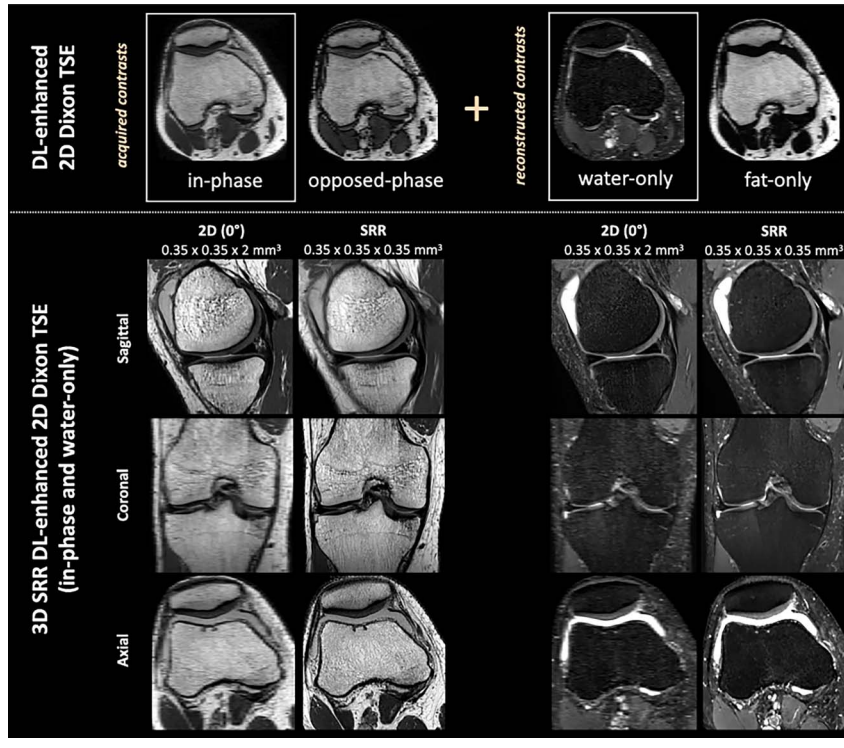

FIGURE 3. DL-enhanced 2D Dixon TSE and 3D SRR Dixon TSE images of a right knee of a 31-year-old male patient volunteer referred for clinical knee MRI due to sustained knee pain and swelling after sports. The DL-enhanced 2D Dixon TSE technique allows to acquire 2 contrasts, that is, in-phase and opposed-phase images, during a single acquisition. From these acquired contrasts, the water-only and fat-only images can be reconstructed. In this study, the 2D in-phase and water-only images were used as input for the SRR algorithm. Three representative slices of the sagittal 2D acquisitions (defined as 0° rotation around the phase-encoding axis) are shown in the sagittal, coronal, and axial orientations, next to their corresponding superresolution reconstructed versions.

artifacts present). The following image characteristics were assessed: overall image quality, subjective SNR, homogeneity of FS, fluid brightness, presence of various artifacts[33] (artifacts related to the image reconstruction process excluding aliasing [ie, reconstruction artifacts], motion, aliasing, chemical shift, and pulsation artifacts), edge sharpness, contrast resolution, and partial volume effects. The anatomical structures considered for the visibility assessment were medial meniscus (MM) and lateral meniscus (LM), patellofemoral and femorotibial articular cartilage, anterior cruciate ligament (ACL) and posterior cruciate ligament (PCL), medial and lateral collateral ligament, tendons of the extensor apparatus, medial quadriceps and gastrocnemius muscles, and bone (femur, tibia, fibula, patella). The presence and location of internal knee derangements, including high-grade cartilage defects (ie, grades 3 and 4 according to the Outerbridge Classification),[34] meniscal tears,[35–37] tears of ligaments,[38] tendons or muscles, and bone injuries, were recorded by the MSK radiologists (readers A and B).[39] Moreover, they assigned a confidence level to their diagnoses by means of an additional 5-point Likert scale[26] (1 = definitely normal; 2 = probably normal; 3 = equivocal; 4 = probably abnormal; 5 = definitely abnormal). In the presence of multiple cartilage defects at different locations, only the dominant high-grade lesion was considered. Ligamentous and musculotendinous tears were recorded if fiber discontinuity was more than 50%. Furthermore, a single occurrence or multiple/combined occurrences of bone marrow edema, cortical fractures, and subchondral fractures were defined as a bone injury.

Upon completion of all readings, the MSK radiologists organized a consensus reading with all available MRI data (including the clinical 2D TSE as standard-of-reference) and patients' clinical findings. This consensus reading served as a reference standard for the MR evaluation of structural abnormalities.[12,17] For the sole 2 patients that underwent knee arthroscopy, the arthroscopic reports were used as reference standard.

Statistical Analysis

All statistical analyses were performed using R (version 4.2.3, R Foundation for Statistical Computing, Vienna, Austria). Statistical significance was defined for P values <0.05. The second readings of the readers were used for data presentation.

The Likert scores for the image quality variables and anatomical visibility of structures were summarized using descriptive statistics (mean, median, and interquartile range) and analyzed with the nonparametric Friedman test. A positive Friedman test (overall P value <0.05) was followed by post hoc testing using the pairwise Wilcoxon signed rank test with Holm correction to identify significant differences in image quality and anatomical visibility between the standard 2D protocol and each research protocol (ie, DL-enhanced accelerated 2D and 3D SRR Dixon).

For the analysis of the diagnostic confidence, scores were dichotomized into definite (1 and 5) and probable (2, 3 and 4) scores to calculate the readers' degree of certainty. Subsequently, repeated McNemar tests with Holm correction were used to compare the degrees of certainty of the standard 2D protocol versus each research protocol for both readers.

Interreader and intrareader agreement were assessed by means of the weighted Fleiss-Cohen kappa (κ) statistic with 95% confidence intervals. κ values were interpretated according to the ranges defined by Landis and Koch[40]: 0–0.20, poor; 0.21–0.40, fair; 0.41–0.60, moderate; 0.61–0.80, substantial; and 0.81–1.00, almost perfect agreement.

Results

Representative images of a comprehensive knee examination illustrating the image quality of the 3 different protocols used in this study are shown in Figure 2. Compared with the original 2D Dixon data, the 3D SRR Dixon images with in-phase and water-only contrasts display a clear improvement of the through-plane resolution on coronal and axial views as shown in Figure 3.

The standard 2D TSE protocol (PAT 2), the DL-enhanced accelerated 2D TSE protocol (PAT 2 × SMS 2), and the accelerated 3D SRR DL-enhanced 2D Dixon TSE protocol (PAT 3 × SMS 2) were successfully applied to all patients, without the need for repeated measurements due to major artifacts. The accelerated 2D and 3D DL-enhanced protocols were 44% faster than the clinical standard 2D TSE protocol (ie, 6 minutes 24 seconds versus 11 minutes 23 seconds).

Image quality

Scores from the image quality assessment are summarized in Table 3. The overall image quality of the standard 2D and DL-enhanced 2D protocols was good to excellent according to all 3 readers. Only for reader B, the standard 2D showed significantly better image quality than the DL-enhanced 2D protocol ($P < 0.01$). The overall image quality of the 3D SRR Dixon protocol was good according to reader A, adequate according to reader B, and poor to adequate for reader C. The standard 2D protocol had significantly better image quality compared with the 3D SRR Dixon protocol for readers B and C ($P < 0.001$ and $P < 0.01$, respectively). Edge sharpness was generally evaluated in the same way as the overall image quality by all readers. The subjective SNR was commonly found to be good for all protocols. Only for reader C, the DL-enhanced 2D images showed a significant improvement in SNR compared with the standard 2D images ($P < 0.01$). Contrast resolution, fluid brightness, and the homogeneity of FS were scored good to excellent by all readers for all protocols. However, for reader A, the Dixon method resulted in a better FS than the fat saturation method used in the standard 2D protocol ($P < 0.05$). In terms of artifacts, distortions due to motion were minimally present or absent for 2D protocols as observed by all readers. Motion artifacts were not directly scored for 3D SRR Dixon images as they were considered under reconstruction artifacts (given that SRR with integrated motion estimation was used). Although little to no reconstruction or aliasing artifacts were recorded for the 2D protocols, all readers observed such artifacts in the 3D SRR Dixon images (Fig. 4). This led to significant differences between the standard 2D and 3D SRR Dixon protocols in terms of the perceived image reconstruction quality ($P < 0.01$ for reader A and $P < 0.001$ for readers B and C) and the presence of aliasing artifacts ($P < 0.001$ for all readers). There was also a significant difference in the reconstruction quality between the two 2D protocols for reader B ($P < 0.001$). According to all readers, banding artifacts were absent and chemical shift effects were minimal for all protocols. Pulsation artifacts and partial volume effects were only mildly present in both 2D protocols and more absent in the 3D SRR images according to all readers. This artifact reduction was significant for 3D SRR Dixon compared with the standard 2D protocol for readers B and C ($P < 0.001$ and $P < 0.01$, respectively).

Anatomical Visibility of Knee Structures

The visibility of all knee structures was good with no significant differences between protocols for reader A. Reader B observed excellent visualization of ligaments, tendons, muscle, and bone and near excellent visualization of menisci and cartilage with standard 2D and DL-enhanced 2D protocols. In addition, reader B graded the visualization of menisci, ligaments, and muscle as near excellent for the 3D SRR Dixon protocol, whereas cartilage was significantly better visible on standard 2D than on 3D SRR Dixon images according to this reader ($P < 0.001$). Tendons and bone showed adequate to good visibility on 3D SRR Dixon images for reader B differing significantly from the standard 2D protocol ($P < 0.001$). The scores of the anatomical visibility evaluation are summarized in Table 4.

Diagnostic Confidence

In general, readers A and B felt equally confident assessing normal and abnormal knee structures with any of the 3 study protocols. However, for the evaluation of cartilage and tendons, reader B recorded

TABLE 2. MRI Parameters of the Clinical and DL-Enhanced Accelerated 2D TSE-Based Protocols

	Axial IW FS		Coronal IW FS		Coronal T1	
Parameter	**Standard**	**Accelerated**	**Standard**	**Accelerated**	**Standard**	**Accelerated**
Repetition time, ms	5060	3030	3560	3900	597	500
Echo time, ms	35	36	36	35	18	6.7
Fat suppression	FatSat	SPAIR	FatSat	SPAIR		
PAT acceleration factor	2	2	2	2	3	2
SMS acceleration factor		2		2		2
Field of view shift factor		2		4		4
Echo train length	7	9	7	11	3	4
Receiver bandwidth, Hz/pixel	148	200	179	301	260	355
Flip angle, °	180	125	150	125	150	121
Averages	1	1	1	1	1	1
Concatenations	1	1	1	1	2	1
Field of view, mm^2	140 × 140	140 × 140	140 × 140	140 × 140	140 × 140	140 × 140
Matrix size	384 × 288	320 × 240	416 × 333	272 × 204	480 × 336	256 × 173
Slice thickness/gap, mm	2.50/0.25	3.00/0.30	3.00/0.30	3.00/0.30	3.00/0.30	3.50/0.35
No. slices	42	38	30	36	30	26
Phase encoding direction	R >> L	R >> L	R >> L	R >> L	R >> L	R >> L
Phase oversampling, %	20	100	60	95	50	140
Enhancement technique	Iter-Den + IP-SR	DL-Den + IP-SR	Iter-Den + IP-SR	DL-Den + IP-SR	Iter-Den + IP-SR	DL-Den + IP-SR
No. repetitions	1	1	1	1	1	1
Angles of rotation, °						
Reconstructed voxel size, mm^3	**0.18 × 0.18 × 2.50**	**0.22 × 0.22 × 3.00**	**0.17 × 0.17 × 3.00**	**0.26 × 0.26 × 3.00**	**0.15 × 0.15 × 3.00**	**0.27 × 0.27 × 3.50**
Total acquisition time, min:s	**02:28**	**01:37**	**02:31**	**01:26**	**01:17**	**00:34**

PAT, parallel acquisition technique; SMS, simultaneous multislice; IW, intermediate-weighted; PD, proton density–weighted; T1, T1-weighted; T2, T2-weighted; FS, fat suppressed; SRR, superresolution reconstruction; FatSat, fat saturation; SPAIR, spectral attenuated inversion recovery; Iter-Den, iterative denoising; DL-Den, deep learning–based denoising; IP-SR, in-plane superresolution; TP-SR, through-plane superresolution.

a lower percentage of definite diagnoses when using 3D SRR Dixon data instead of the standard 2D protocol. This only reached significance for the evaluation of tendons ($P < 0.01$). An overview of the readers' degree of certainty based on the diagnostic confidence scores for all protocols is provided in Table 5.

Among the 16 patients enrolled in the main study, the occurrence of structural abnormalities compliant with the study's lesion inclusion criteria was as follows: 11 cartilage lesions (medial femoral condyle, n = 2; medial tibial plateau, n = 1; lateral tibial plateau, n = 2; trochlea, n = 2; patella, n = 4), 9 meniscus lesions (medial meniscus, n = 4; lateral meniscus, n = 5), 6 ACL lesions, and 11 bone injuries (femoral, n = 4; tibial, n = 5; patellar, n = 2).

Based on the consensus reading, all bone injuries and ligamentous lesions (ACL derangements) were correctly identified with the highest degree of certainty by both readers with all protocols. Only for 1 patient, reader A did not report a femoral subchondral fracture with the 3D SRR Dixon protocol. An example of a subchondral fracture with surrounding bone marrow edema is shown in Figure 5. In addition, 2 representative ACL injuries following acute knee trauma are shown in Figure 6, in which all 2D FS and 3D SRR water-only images nicely depict the discontinuity of ACL fibers, whereas the reformatted parasagittal and paracoronal 3D SRR images allow for an improved visualization of lesion location and extension.

Looking at the meniscal injuries, 7 out of 9 lesions confirmed by consensus were recorded by both readers with all protocols. An example of an MM tear that was subsequently arthroscopically confirmed is shown in Figure 7A. One small radial LM tear was missed in all images by both readers during the second reading but observed with the standard 2D protocol (scored as probably abnormal by reader B) and 3D SRR Dixon protocol (scored as definitely abnormal by readers A and B) during the first reading. Another subtle radial LM lesion was fully missed by reader A, whereas it was observed with all protocols by the other reader. Besides the meniscal lesions confirmed by consensus, 4 clinically suspected cases of MM injury, only seen on 3D SRR Dixon images, were documented. In 3 of these 4 cases, only 1 reader identified a lesion (once reader A, and twice reader B), whereas in the other case, both readers identified an abnormality with the 3D SRR Dixon protocol. Two suspicious MM lesions, equivocal on 3D SRR Dixon MRI, could not be confirmed on the 2D reference images, 1 case was caused by meniscal flounce,[37] and 1 MM lesion appeared equivocal on the reference 2D while showing as a definite grade 3 tear on 3D SRR Dixon images. The latter case is displayed in Figure 7B.

TABLE 2. MRI Parameters of the Clinical and DL-Enhanced Accelerated 2D TSE-Based Protocols, Continued

	Sagittal PD		Sagittal T2 FS		Sagittal IW Dixon
Parameter	**Standard**	**Accelerated**	**Standard**	**Accelerated**	**Accelerated 3D SRR**
Repetition time, ms	2990	3000	4070	3480	4190
Echo time, ms	19	15	64	53	40
Fat suppression			FatSat	SPAIR	Dixon
PAT acceleration factor	2	2	2	2	3
SMS acceleration factor		2		2	2
Field of view shift factor		4		4	4
Echo train length	7	11	11	11	16
Receiver bandwidth, Hz/pixel	222	354	252	201	606
Flip angle, °	180	125	180	125	120
Averages	1	1	2	1	1
Concatenations	1	1	1	1	1
Field of view, mm^2	140 × 140	140 × 140	140 × 140	140 × 140	136 × 136
Matrix size	512 × 384	336 × 252	336 × 252	304 × 228	192 × 192
Slice thickness/gap, mm	2.50/0.25	3.00/0.30	2.50/0.25	3.00/0.30	2.00/0
No. slices	35	38	35	38	62
Phase encoding direction	H >> F	H >> F	H >> F	H >> F	H >> F
Phase oversampling, %	70	100	50	100	50
Enhancement technique	Iter-Den + IP-SR	DL-Den + IP-SR	Iter-Den + IP-SR	DL-Den + IP-SR	DL-Den + IP-SR + TP-SR
No. repetitions	1	1	1	1	6
Angles of rotation, °					0, 30, 60, 90, 120, 150
Reconstructed voxel size, mm^3	**0.14 × 0.14 × 2.50**	**0.21 × 0.21 × 3.00**	**0.21 × 0.21 × 2.50**	**0.23 × 0.23 × 3.00**	**0.35 × 0.35 × 0.35**
Total acquisition time, min:s	**02:31**	**01:21**	**02:36**	**01:26**	**06:24**

PAT, parallel acquisition technique; SMS, simultaneous multislice; IW, intermediate-weighted; PD, proton density–weighted; T1, T1-weighted; T2, T2-weighted; FS, fat suppressed; SRR, superresolution reconstruction; FatSat, fat saturation; SPAIR, spectral attenuated inversion recovery; Iter-Den, iterative denoising; DL-Den, deep learning–based denoising; IP-SR, in-plane superresolution; TP-SR, through-plane superresolution.

Despite the wider range of confidence scores for the evaluation of cartilage (ie, 56.2%–100%, Table 5), 8 out of 11 cartilage lesions were identified by all readers with all protocols. Two examples of articular cartilage defects well depicted with all protocols are shown in Figure 8. The cases with disagreement included 2 lesions confirmed by consensus that were fully missed by reader B but recorded by reader A on standard 2D and DL-enhanced 2D images, respectively. A third lesion was not documented by reader A, whereas it was detected by reader B using each protocol.

Interreader and Intrareader Agreement

In general, the interreader and intrareader agreement for the assessment of internal knee derangements using any of the 3 protocols was substantial to almost perfect with κ values ranging between 0.67 and 1.00.

Regarding the assessment of cartilage, interreader agreement was substantial for DL-enhanced 2D and almost perfect for standard 2D and 3D SRR Dixon protocols (κ values of 0.79, 0.98, and 0.87, respectively). The intrareader agreement of both readers for cartilage assessment was almost perfect for all protocols (κ values of 0.89–0.94 for reader A and 0.90–0.99 for reader B). For the evaluation of menisci, interreader agreement was substantial for 3D SRR Dixon (κ values of 0.70–0.80) and for the LM on standard 2D images (κ value of 0.80). It was almost perfect for the MM on standard 2D images (κ value of 0.99) and the DL-enhanced 2D protocol (κ values of 0.87–1.00). Intrareader agreement on menisci assessment was higher for both 2D protocols but remained substantial to almost perfect for the 3D SRR Dixon protocol (κ values of 0.80–0.89 for reader A, and κ values of 0.67–0.75 for reader B). No reader differences were found for the assessment of the ACL resulting in an overall κ value of 1.00. Finally, interreader agreement on bone injuries was almost perfect for all protocols (0.86–1.00), whereas the intrareader agreement of reader A (κ values of 0.73–0.86) was overall lower than the intrareader agreement of reader B (κ values of 0.99–1.00).

The weighted Fleiss-Cohen κ values for the interreader and intrareader agreement are provided in Table 6.

Discussion

In this study, we investigated the use of a DL-enhanced 4-fold accelerated 2D TSE protocol for rapid 2D knee MRI and the feasibility of a novel 3D SRR Dixon TSE protocol for accelerated comprehensive 3D knee MRI, by comparing their image quality characteristics and

TABLE 3. Image Quality Scores

	Protocol	Overall Image Quality	Edge Sharpness	Subjective SNR	Contrast	Fluid Brightness	Fat Suppression
Reader A	Standard 2D	3,94 [4 (4–4)]	3,88 [4 (4–4)]	3,94 [4 (4–4)]	4 [4 (4–4)]	4,06 [4 (4–4)]	4 [4 (4–4)]
	DL-enhanced 2D	3,94 [4 (4–4)]	3,94 [4 (4–4)]	3,94 [4 (4–4)]	4 [4 (4–4)]	4 [4 (4–4)]	4 [4 (4–4)]
	3D SRR Dixon	3,81 [4 (4–4)]	3,81 [4 (3–4)]	3,75 [4 (3,75–4)]	4,25 [4 (4–4,25)]	4,38 [4 (4–5)]	4,38 [4 (4–5)]*
Reader B	Standard 2D	4,56 [5 (4–5)]	4,63 [5 (4–5)]	4 [4 (4–4)]	5 [5 (5–5)]	5 [5 (5–5)]	4,94 [5 (5–5)]
	DL-enhanced 2D	4 [4 (4–4)]**	4 [4 (4–4)]**	4 [4 (4–4)]	5 [5 (5–5)]	5 [5 (5–5)]	5 [5 (5–5)]
	3D SRR Dixon	2,88 [3 (3–3)]***	2,94 [3 (3–3)]***	4 [4 (4–4)]	5 [5 (5–5)]	5 [5 (5–5)]	5 [5 (5–5)]
Reader C	Standard 2D	4,06 [4 (3,75–5)]	4,06 [4 (3–5)]	3,5 [3 (3–4)]	4,25 [4 (4–5)]	5 [5 (5–5)]	4,19 [4 (4–4)]
	DL-enhanced 2D	4,56 [5 (4–5)]	4,56 [5 (4–5)]	4,69 [5 (4–5)]**	4,69 [5 (4–5)]	5 [5 (5–5)]	4,06 [4 (4–4)]
	3D SRR Dixon	2,5 [2,5 (2–3)]**	2,63 [3 (2–3)]**	3,81 [4 (3,75–4)]	4,5 [4,5 (4–5)]	5 [5 (5–5)]	4,38 [4 (4–5)]

Likert scores of the image quality variables reported as mean [median (interquartile range)]. Statistically significant P values are defined as follows: *$P < 0.05$, **$P < 0.01$, ***$P < 0.001$. Motion artifacts were not scored for 3D SRR Dixon images as an SRR method with integrated motion estimation was used.

SRR, superresolution reconstruction; SNR, signal-to-noise ratio.

diagnostic performance to conventional 2-fold accelerated 2D TSE knee MRI. Overall, the evaluated research protocols performed similarly to the conventional 2D TSE protocol while enabling a considerable reduction in scan time. To the best of our knowledge, this is the first study to evaluate the feasibility of comprehensive multicontrast DL-enhanced (ie, DL-based denoising and in-plane SRR) PI and SMS accelerated 2D TSE and 3D SRR Dixon knee protocols, and the first time a DL-enhanced PI and SMS accelerated TSE sequence with Dixon functionality is used to this end. The 3D SRR technique was included in the comparison as it mimics the familiar 2D TSE contrasts more closely than commercially available direct 3D MRI sequences.[23,41]

The presented 3D SRR Dixon TSE protocol deals with the limitations of the previously reported 3D SRR acquisition protocol for knee MRI by exploiting the acceleration potential of the WIP 2D TSE sequence (ie, SRR input) that allows for the combined use of PI and SMS accelerations with DL-reconstruction and Dixon FS.[23] Where previously only a single (IW) contrast could be obtained in a total scan time of 13 minutes 25 seconds, the novel SRR protocol can provide up to 4 different contrasts in less than half of this reported time. Although only in-phase and water-only images were retained for subsequent through-plane SRR in this study, fat-only images that are an alternative for the T1-weighted contrast can also be used as input for the SRR. Although not required for the intended evaluation,[1,42] 3D SRR fat-only images should be included in future validation studies for the detection of fractures and bone marrow infiltration processes (eg, infection or tumor).

Another limitation of the previous 3D SRR knee MRI protocol, that is, lower image contrast and fluid brightness compared with conventional 3D SPACE acquisitions, was addressed in the novel 3D SRR protocol by using optimized DL-enhanced 2D Dixon IW TSE acquisitions as input data, achieving good to excellent contrast resolution and fluid brightness comparable to standard 2D TSE MRI.

Moreover, the synergy of the offline through-plane SRR and the inline DL-based in-plane SRR resulted in a higher spatial resolution than previously reported (ie, $0.35 \times 0.35 \times 0.35$ mm^3 compared with $0.50 \times 0.50 \times 0.50$ mm^3). The resolution increase in the slice-encoding direction was achieved with an SRR method based on a rotated acquisition scheme instead of a shifted one as it was previously demonstrated that rotated schemes lead to higher accuracy and precision of the SRR.[43] The number of rotated 2D IW Dixon TSE slice stacks used in this study was heuristically set to 6 as this provided a good trade-off between the total acquisition time and image quality. However, as this number is lower than the optimal number of rotations to effectively cover the k-space (ie, 9 rotations),[44] the effective through-plane resolution of the 3D SRR data may be lower than 0.35 mm. Furthermore, as the 3D SRR images were compared with standard 2D TSE data with overall higher in-plane resolution, edge sharpness was evaluated significantly lower for the 3D SRR Dixon TSE protocol. Nevertheless, the reconstructed voxel volume of the 3D SRR data was 1.15 and 3 times smaller compared with the smallest voxel volume acquired with the 2D standard and DL-enhanced accelerated 2D TSE protocol respectively, without any differences in subjective SNR. The 3D SRR voxel volume is also smaller than commonly reported voxel volumes acquired with accelerated 3D knee MRI sequences.[21,23,45]

Despite the aforementioned improvements, the 3D SRR Dixon TSE datasets exhibited noticeable aliasing and reconstruction artifacts.

The DL-enhanced 6-fold accelerated 2D IW Dixon TSE acquisitions, used as input for the through-plane SRR, displayed aliasing artifacts because of the parameter configuration, and in particular the higher acceleration factors, used to match the acquisition time of the DL-enhanced 4-fold accelerated 2D protocol (Fig. 4). Consequently, aliasing artifacts were significantly more present in bone on the 3D SRR Dixon TSE images, as observed by all readers (Table 3). Although these artifacts were not markedly present when setting up the 3D SRR Dixon TSE protocol in a test volunteer, they were present in most of the 3D SRR images in this study but did not affect the diagnostic confidence or performance further on.

Aliasing artifacts in the accelerated 2D IW Dixon TSE acquisitions could be fully avoided by increasing the oversampling in the phase-encoding direction. This would result in a slightly prolonged acquisition (approximately 1 minute extra) but would still provide a significant time gain compared with standard 2D TSE knee MRI.

The 3D SRR data also suffered from reconstruction artifacts due to the limited number of rotated slice stacks used. These artifacts, observed by all readers (Table 3), mainly manifested as parallel streaks at the periphery of the knee joint (Fig. 4), impacting the visibility and diagnostic confidence for the assessment of the extensor tendons and patellofemoral cartilage. These artifacts can be mitigated by acquiring additional slice-rotated 2D Dixon IW TSE input volumes and/or performing the SRR to a high-resolution grid with lower through-plane resolution (eg, 0.53 mm).

Despite the substantial to almost perfect interreader agreement for the assessment of internal knee derangements by the 2 radiologists, there was a marked difference between the scores of reader A and the scores of readers B and C (which displayed similar trends) for multiple image quality variables, particularly for the assessment of the 3D SRR Dixon TSE protocol (Table 3). This divergence in assessment could be explained by the greater experience of the senior radiologist (reader A) with 3D MRI and 3D SRR MRI, the more recent introduction of reader B to 3D techniques and the different, more technical background of reader C. Nevertheless, the lower overall image quality perceived by reader B for the 3D SRR

TABLE 3. Image Quality Scores, Continued

Motion	Reconstruction	Aliasing	Banding	Chemical Shift	Pulsation	Partial Volume Effect
3,81 [4 (4–4)]	4 [4 (4–4)]	5 [5 (5–5)]	5 [5 (5–5)]	4 [4 (4–4)]	4 [4 (4–4)]	4 [4 (4–4)]
3,88 [4 (4–4)]	3,94 [4 (4–4)]	5 [5 (5–5)]	5 [5 (5–5)]	4 [4 (4–4)]	3,81 [4 (4–4)]	4 [4 (4–4)]
	3,25 [3 (3–3,25)]**	3,88 [4 (4–4)]***	5 [5 (5–5)]	4 [4 (4–4)]	4 [4 (4–4)]	4,19 [4 (4–4)]
4,56 [5 (4–5)]	5 [5 (5–5)]	5 [5 (5–5)]	5 [5 (5–5)]	4 [4 (4–4)]	4 [4 (4–4)]	4,06 [4 (4–4)]
4,5 [4,5 (4–5)]	4,13 [4 (4–4)]***	5 [5 (5–5)]	5 [5 (5–5)]	4 [4 (4–4)]	4 [4 (4–4)]	4,06 [4 (4–4)]
	2,75 [3 (2,75–3)]***	3,31 [3 (3–4)]***	5 [5 (5–5)]	4 [4 (4–4)]	5 [5 (5–5)]***	5 [5 (5–5)]***
4,38 [5 (3,75–5)]	4,63 [5 (4–5)]	5 [5 (5–5)]	5 [5 (5–5)]	4 [4 (4–4)]	3,81 [4 (4–4)]	3,94 [4 (4–4)]
4,63 [5 (4–5)]	4,75 [5 (4,75–5)]	4,94 [5 (5–5)]	5 [5 (5–5)]	4 [4 (4–4)]	3,81 [4 (4–4)]	3,88 [4 (4–4)]
	2,25 [2 (2–2,25)]***	3,19 [3 (3–3)]***	5 [5 (5–5)]	4 [4 (4–4)]	4,63 [5 (4–5)]**	4,75 [5 (5–5)]**

Likert scores of the image quality variables reported as mean [median (interquartile range)]. Statistically significant P values are defined as follows: *$P < 0.05$, **$P < 0.01$, ***$P < 0.001$. Motion artifacts were not scored for 3D SRR Dixon images as an SRR method with integrated motion estimation was used.

SRR, superresolution reconstruction; SNR, signal-to-noise ratio.

protocol was not reflected in the diagnostic confidence scores for the evaluation of knee structures, except for cartilage and tendon.

The anatomical visibility of menisci was good to excellent for all 2D and 3D protocols. Yet, the degree of diagnostic certainty for both readers was slightly (but not significantly) lower for evaluating MM on 3D SRR Dixon TSE images, also leading to a lower interreader agreement and intrareader agreement for reader B compared with the 2D protocols. These results are related to the 4 clinically suspected cases of MM lesions, which could only be well observed with the 3D SRR Dixon protocol but could not be strictly confirmed during the consensus reading. Despite the pronounced pathological appearance of some of these medial menisci on 3D SRR images (eg, Fig. 7B), a more elaborate investigation with arthroscopic correlation in a larger patient cohort is needed to evaluate the sensitivity of the 3D SRR Dixon protocol to MM lesions.

In addition, and even though the accelerated 2D protocol obtained almost perfect agreement for LM lesions, the relatively lower κ values both for the interreader and intrareader evaluations indicate that LM lesions are in general more difficult to read consistently than MM lesions (Table 6).[46]

Both the anatomic visibility and the diagnostic confidence scores of cartilage were generally lower when compared with the other

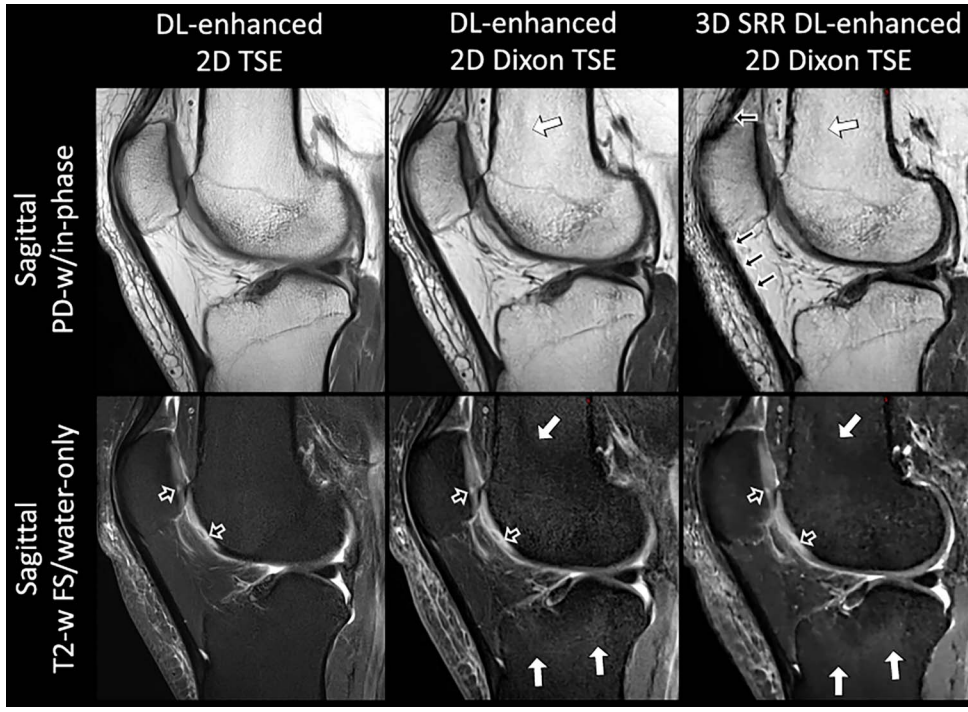

FIGURE 4. Left knee of a 44-year-old male patient presented with knee locking. 2D T2-weighted FS, 2D water-only, and 3D SRR water-only sagittal views display patellar and trochlear chondral defects (small black arrows). Aliasing artifacts can be observed for DL-enhanced 2D Dixon TSE (ie, SRR input) and 3D SRR Dixon TSE images due to insufficient phase-oversampling (white arrows). These artifacts are especially visible in 3D SRR water-only images but were found to not affect the data's clinical usability. DL-enhanced 2D TSE images generally did not suffer from aliasing artifacts as more phase oversampling was used. Line artifacts, denoted as reconstruction artifacts, across the patellar and quadriceps tendons can be observed on 3D SRR in-phase images (large black arrows). In addition, the extensor tendon region has a blurrier appearance on 3D SRR Dixon TSE images, which resulted in a lower diagnostic confidence for 1 reader.

TABLE 4. Anatomical Visibility Scores

	Protocol	Cartilage	Menisci	Ligaments	Tendons	Muscle	Bone
Reader A	Standard 2D	3,94 [4 (4–4)]	3,88 [4 (4–4)]	4 [4 (4–4)]	4 [4 (4–4)]	4 [4 (4–4)]	4 [4 (4–4)]
	DL-enhanced 2D	3,94 [4 (4–4)]	4 [4 (4–4)]	4 [4 (4–4)]	4 [4 (4–4)]	4 [4 (4–4)]	4 [4 (4–4)]
	3D SRR Dixon	3,88 [4 (3,75–4)]	4,19 [4 (4–4,25)]	4,13 [4 (4–4)]	4,13 [4 (4–4)]	4,13 [4 (4–4)]	4,13 [4 (4–4)]
Reader B	Standard 2D	4,88 [5 (5–5)]	4,94 [5 (5–5)]	5 [5 (5–5)]	5 [5 (5–5)]	5 [5 (5–5)]	5 [5 (5–5)]
	DL-enhanced 2D	4,94 [5 (5–5)]	5 [5 (5–5)]	5 [5 (5–5)]	5 [5 (5–5)]	5 [5 (5–5)]	5 [5 (5–5)]
	3D SRR Dixon	2,56 [3 (2–3)]***	4,94 [5 (5–5)]	4,94 [5 (5–5)]	3,69 [4 (3–4)]***	5 [5 (5–5)]	3,88 [4 (4–4)]***

Likert scores of the anatomical visibility assessment reported as mean [median (interquartile range)]. Statistically significant P value is defined as ***$P < 0.001$.
SRR, superresolution reconstruction.

structures. Interestingly, reader A felt more confident evaluating cartilage on the 3D SRR Dixon images and less confident on the DL-enhanced accelerated 2D images, whereas the opposite was observed for reader B. These differences were captured by a reduced interreader agreement for the DL-enhanced 2D protocol, which has also been noted in a previous study.[14]

Furthermore, reader B assigned significantly lower anatomical visibility scores to bone (due to aliasing artifacts) and to tendon (due to reconstruction artifacts at the extensor tendons) for the 3D SRR images. However, the aliasing did not affect the diagnostic confidence scores of bone for reader B, whereas the reconstruction artifacts did lead to a reduced confidence for tendon assessment (Table 5). In addition, despite assigning excellent confidence to the assessment of bone with all protocols, reader A missed 1 bone lesion on 3D SRR Dixon despite recording this lesion during the first reading.

There were several limitations to this study. First, the evaluated protocols had different in- and through-plane resolutions. These resolution differences were due to the diverse origins of the protocols; the conventional 2D TSE protocol was the unmodified in-house protocol for routine knee examination, the DL-enhanced accelerated 2D TSE protocol was configured according to Fritz et al and Del Grande et al,[2,8] and the 3D SRR Dixon TSE protocol was tuned to match the acquisition time of the DL-enhanced 2D protocol. In addition, all protocols used a different FS technique.

The aforementioned differences, partly inherent to the subject of our investigation, may have allowed the readers to recognize the type of image protocol, potentially introducing a recognition bias in their assessments due to personal preferences.

A second limitation of the study is the lack of an arthroscopic reference to confirm the identified findings. There were only 2 patients with available arthroscopic data, obtained outside of the current study. These data were used to confirm a clear definite MM lesion and a cartilage lesion. However, previous studies have shown that a radiologists' consensus reading, as carried out in this study, is a valuable alternative golden standard for the diagnostic evaluations.[12,17]

Third, the study's sample size was relatively small, and consequently, the pathological findings were recorded in a limited number of knee structures. Nevertheless, it was possible to observe significant differences in the outcome variables and to illustrate the diagnostic potential of the accelerated research protocols.

Finally, the 3D SRR Dixon TSE protocol was not compared with other commercially available accelerated 3D sequences such as 3D CAIPIRINHA SPACE and 3D CS TSE MRI[23,41] as these are not as widely adopted as accelerated 2D TSE protocols for knee MRI in the clinical routine.[22,45] Moreover, scan time constraints to guarantee patient comfort limited the number of protocols included in the study.

Given the advantages of 3D MRI compared with 2D acquisitions and the ongoing developments of 3D knee MRI regarding acceleration and image quality enhancement by means of DL algorithms,[45,47] future work should assess the diagnostic performance of an optimized 3D SRR Dixon TSE protocol and other DL-enhanced accelerated 3D protocols with arthroscopic correlation in a large patient cohort.

TABLE 5. Diagnostic Confidence Scores

	Reader A			Reader B		
	% Certainty			% Certainty		
Structure	Standard 2D	DL-Enhanced 2D	3D SRR Dixon	Standard 2D	DL-Enhanced 2D	3D SRR Dixon
Cartilage	75	68.75	93.75	87.5	100	56.25
MM	93.75	100	81.25	100	100	87.5
LM	93.75	93.75	93.75	100	93.75	100
MCL	100	100	100	100	100	100
LCL	100	100	100	100	100	100
ACL	100	100	100	100	100	100
PCL	100	100	100	100	100	100
Tendons	100	100	100	100	100	56.25**
Muscle	100	100	100	100	100	100
Bone	100	100	100	100	100	100

Readers A and B assigned a confidence level to their diagnoses with a 5-point Likert scale. These scores were dichotomized into definite (1 and 5) and probable (2, 3, and 4) scores to calculate the percentage of definite diagnoses, that is, the percentage certainty. Statistically significant P value is defined as follows: **$P < 0.01$.

SRR, superresolution reconstruction; MM, medial meniscus; LM, lateral meniscus; MCL, medial collateral ligament; LCL, lateral collateral ligament; ACL, anterior cruciate ligament; PCL, posterior cruciate ligament.

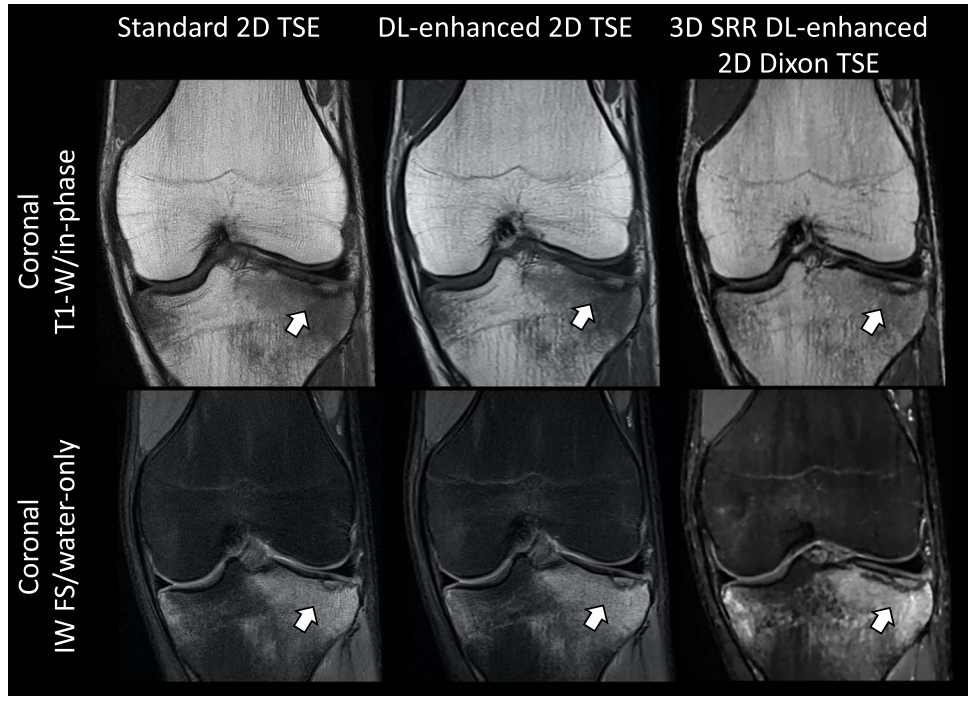

FIGURE 5. Left knee of 18-year-old male patient who suffered a skiing trauma. A nondisplaced subchondral fracture with surrounding bone marrow edema at the lateral tibial plateau can be well observed on all 2D T1-weighted and 3D SRR in-phase coronal views, and on 2D IW FS and 3D SRR water-only images. The latter display comparable contrasts despite the different fat suppression techniques used.

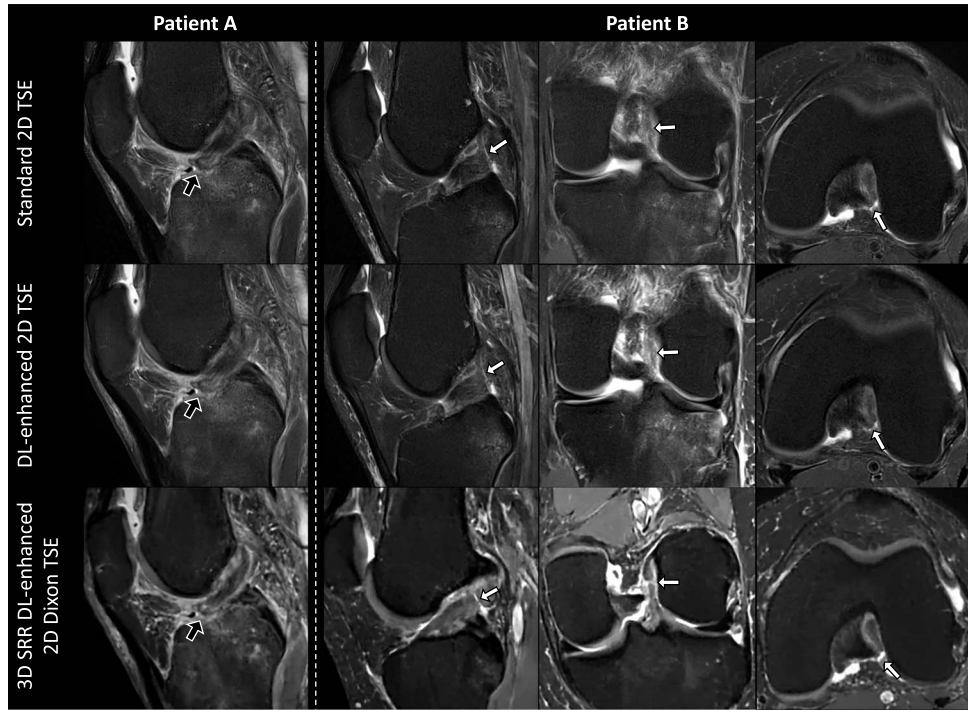

FIGURE 6. A, Left knee of a 57-year-old female patient and B, Left knee of a 41-year-old female patient (both skiing traumas). 2D sagittal T2-weighted FS and 3D SRR water-only images of patient A show a distal ACL injury (black arrows). Images of patient B display a proximal ACL tear (white arrows), which is better visualized on the reformatted parasagittal and paracoronal 3D SRR water-only images (bottom row) than on the sagittal and coronal standard 2D and DL-enhanced 2D images. 2D and 3D SRR axial images depict the tear equally well (white arrows).

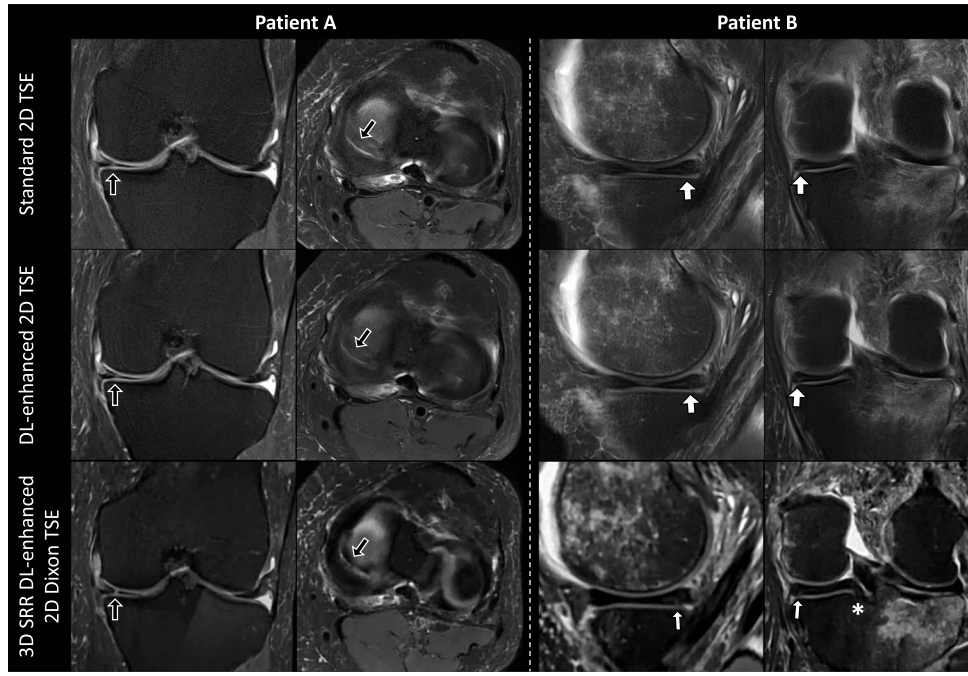

FIGURE 7. A, Left knee of a 50-year-old female patient with chronic knee pain. B, Left knee of a 57-year-old female patient with a recent ski-related knee injury. 2D coronal and axial IW FS and 3D SRR water-only images of patient A show a tear of the medial meniscus extending near the meniscal root (black arrows). This lesion was arthroscopically confirmed. For patient B, 3D SRR water-only images show signs of a definite grade 3 medial meniscus tear (thin white arrows), whereas this is equivocal on 2D sagittal T2-weighted FS and 2D coronal IW FS images (thick white arrows). Moreover, 3D SRR coronal images excellently depict the posteromedial meniscal root insertion (white asterisk).

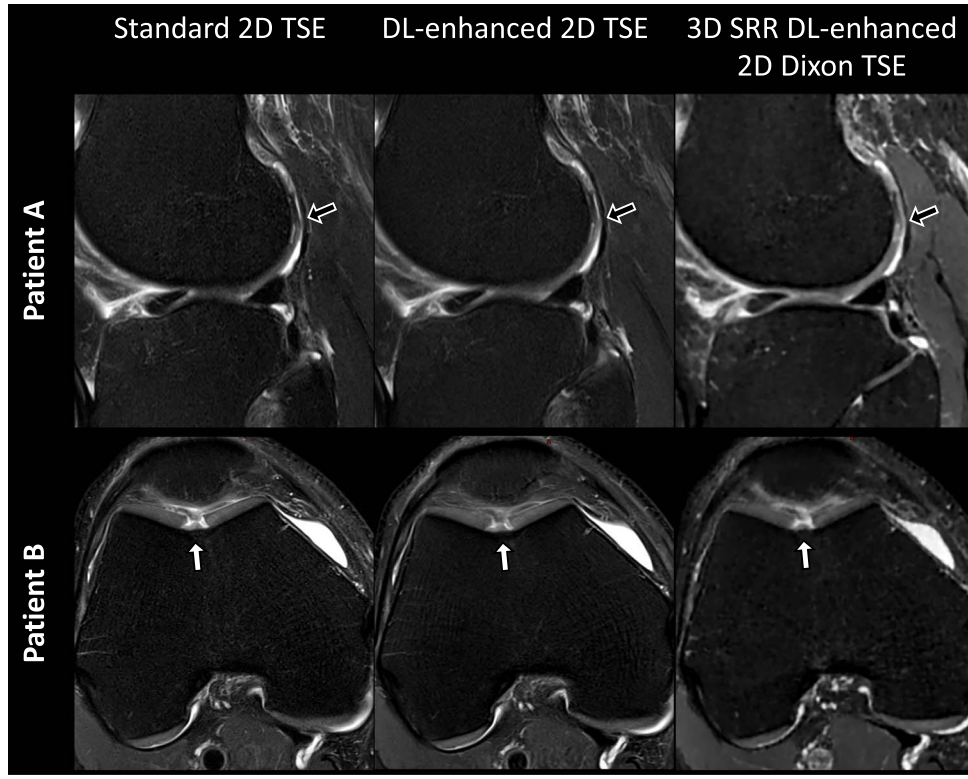

FIGURE 8. A, Left knee of a 51-year-old female patient and B, Right knee of a 31-year-old male patient, both presenting with chronic knee pain. Sagittal images of patient A show cartilage delamination at the posterior aspect of the lateral femoral condyle. This is equally well distinguishable on 2D (DL-enhanced) T2-weighted FS images as on 3D SRR water-only images. For patient B, a shouldered trochlear cartilage defect can be well observed on both 2D IW FS and 3D SRR water-only axial images.

TABLE 6. Interreader and Intrareader Agreement for Assessment of Structural Abnormalities

	Interreader Agreement						Intrareader Agreement—Reader A						Intrareader Agreement—Reader B					
	Standard 2D		DL-Enhanced 2D		3D SRR Dixon		Standard 2D		DL-Enhanced 2D		3D SRR Dixon		Standard 2D		DL-Enhanced 2D		3D SRR Dixon	
Structure	κ	95% CI	κ	95% CI	κ	95% CI	κ	95% CI	κ	95% CI	κ	95% CI	κ	95% CI	κ	95% CI	κ	95% CI
Cartilage	0.98	0.96 1.00	0.79	0.56 1.00	0.87	0.71 1.00	0.94	0.86 1.00	0.91	0.82 1.00	0.89	0.74 1.00	0.98	0.96 1.00	0.99	0.98 1.00	0.90	0.80 1.00
MM	0.99	0.96 1.00	1.00	1.00 1.00	0.70	0.38 1.00	0.97	0.93 1.00	0.99	0.96 1.00	0.89	0.68 1.00	1.00	1.00 1.00	0.99	0.96 1.00	0.75	0.42 1.00
LM	0.80	0.44 1.00	0.87	0.64 1.00	0.80	0.44 1.00	0.83	0.56 1.00	0.87	0.63 1.00	0.80	0.44 1.00	0.73	0.35 1.00	0.88	0.65 1.00	0.67	0.24 1.00
ACL	1.00	1.00 1.00	1.00	1.00 1.00	1.00	1.00 1.00	1.00	1.00 1.00	1.00	1.00 1.00	1.00	1.00 1.00	1.00	1.00 1.00	1.00	1.00 1.00	1.00	1.00 1.00
Bone	1.00	1.00 1.00	1.00	1.00 1.00	0.86	0.60 1.00	0.86	0.60 1.00	0.74	0.41 1.00	0.73	0.39 1.00	1.00	1.00 1.00	1.00	1.00 1.00	0.99	0.97 1.00

The interreader agreement between readers A and B and the intrareader agreement between both reading sessions of readers A and B are given by the weighted Fleiss-Cohen κ statistic with 95% confidence intervals (CIs).

SRR, superresolution reconstruction; MM, medial meniscus; LM, lateral meniscus; ACL, anterior cruciate ligament.

In conclusion, the presented DL-enhanced 4-fold accelerated 2D TSE protocol provides image quality and diagnostic performance similar to the standard 2D protocol. In addition, 3D SRR of DL-enhanced 6-fold accelerated 2D Dixon TSE MRI is feasible for multicontrast 3D knee MRI as it provides comparable diagnostic performance to standard 2-fold accelerated 2D knee MRI. However, reconstruction and aliasing artifacts need to be further addressed to guarantee a reliable visualization of cartilage, tendons, and bone. Both the 2D and 3D SRR DL-enhanced protocols enable a 44% faster examination compared with conventional 2-fold accelerated routine 2D TSE knee MRI and thus open new paths for more efficient clinical 2D and 3D knee MRI.

ACKNOWLEDGMENTS

The authors thank Dominik Nickel and Thomas Benkert from Siemens Healthineers for providing the research software package "WIP 1062_iTSE."

REFERENCES

1. Schnaiter JW, Roemer F, McKenna-Kuettner A, et al. Diagnostic accuracy of an MRI protocol of the knee accelerated through parallel imaging in correlation to arthroscopy. *RoFo*. 2018;190:265–272.
2. Fritz J, Guggenberger R, Del Grande F. Rapid musculoskeletal MRI in 2021: clinical application of advanced accelerated techniques. *Am J Roentgenol*. 2021;216:718–733.
3. Tuite MJ, Gyftopoulus S, Highmore K, et al. Practice parameter for the performance and interpretation of magnetic resonance imaging (MRI) of the knee. 2020;31:1–16. https://www.acr.org/-/media/ACR/Files/Practice-Parameters/mr-knee.pdf.
4. Parkar AP, Adriaensen MEAPM. ESR essentials: MRI of the knee—practice recommendations by ESSR. *Eur Radiol* Published online 2024. doi:10.1007/s00330-024-10706-7.
5. Altahawi F, Pierce J, Aslan M, et al. 3D MRI of the knee. *Semin Musculoskelet Radiol*. 2021;25:455–467.
6. Kim S, Park C, Kim KS, et al. Clinical feasibility of simultaneous multislice acceleration in knee MRI. *Clin Imaging*. 2022;82:216–223.
7. Matcuk GR, Gross JS, Fields BKK, et al. Compressed sensing MR imaging (CS-MRI) of the knee: assessment of quality, inter-reader agreement, and acquisition time. *Magn Reson Med Sci*. 2020;19:254–258.
8. Del Grande F, Rashidi A, Luna R, et al. Five-minute five-sequence knee MRI using combined simultaneous multislice and parallel imaging acceleration: comparison with 10-minute parallel imaging knee MRI. *Radiology*. 2021;299:635–646.
9. Fritz J, Fritz B, Zhang J, et al. Simultaneous multislice accelerated turbo spin echo magnetic resonance imaging: comparison and combination with in-plane parallel imaging acceleration for high-resolution magnetic resonance imaging of the knee. *Invest Radiol*. 2017;52:529–537.
10. Herrmann J, Koerzdoerfer G, Nickel D, et al. Feasibility and implementation of a deep learning MR reconstruction for TSE sequences in musculoskeletal imaging. *Diagnostics*. 2021;11:1484.
11. Recht MP, Zbontar J, Sodickson DK, et al. Using deep learning to accelerate knee MRI at 3 T: results of an interchangeability study. *Am J Roentgenol*. 2020;215:1421–1429.
12. Lee J, Jung M, Park J, et al. Highly accelerated knee magnetic resonance imaging using deep neural network (DNN)–based reconstruction: prospective, multireader, multi-vendor study. *Sci Rep*. 2023;13:17264.
13. Lin DJ, Walter SS, Fritz J. Artificial intelligence–driven ultra-fast superresolution MRI. *Invest Radiol*. 2023;58:28–42.
14. Herrmann J, Keller G, Gassenmaier S, et al. Feasibility of an accelerated 2D-multi-contrast knee MRI protocol using deep-learning image reconstruction: a prospective intraindividual comparison with a standard MRI protocol. *Eur Radiol*. 2022;32:6215–6229.
15. Johnson PM, Lin DJ, Zbontar J, et al. Deep learning reconstruction enables prospectively accelerated clinical knee MRI. *Radiology*. 2023;307:e220425.
16. Terzis R, Dratsch T, Hahnfeldt R, et al. Five-minute knee MRI: an AI-based super resolution reconstruction approach for compressed sensing. A validation study on healthy volunteers. *Eur J Radiol*. 2024;175:111418.
17. Kim M, Lee S-M, Park C, et al. Deep learning–enhanced parallel imaging and simultaneous multislice acceleration reconstruction in knee MRI. *Invest Radiol*. 2022;57:826–833.
18. Garwood ER, Recht MP, White LM. Advanced imaging techniques in the knee: benefits and limitations of new rapid acquisition strategies for routine knee MRI. *Am J Roentgenol*. 2017;209:552–560.
19. Notohamiprodjo M, Horng A, Kuschel B, et al. 3D-imaging of the knee with an optimized 3D-FSE-sequence and a 15-channel knee-coil. *Eur J Radiol*. 2012; 81:3441–3449.

20. Fritz J, Fritz B, Thawait GG, et al. Three-dimensional CAIPIRINHA SPACE TSE for 5-minute high-resolution MRI of the knee. *Invest Radiol*. 2016;51:609–617.
21. Fritz J, Raithel E, Thawait GK, et al. Six-fold acceleration of high-spatial resolution 3D SPACE MRI of the knee through incoherent k-space undersampling and iterative reconstruction—first experience. *Invest Radiol*. 2016;51:400–409.
22. Van Dyck P, Smekens C, Roelant E, et al. 3D CAIPIRINHA SPACE versus standard 2D TSE for routine knee MRI: a large-scale interchangeability study. *Eur Radiol*. 2022;32:6456–6467.
23. Del Grande F, Delcogliano M, Guglielmi R, et al. Fully automated 10-minute 3D CAIPIRINHA SPACE TSE MRI of the knee in adults: a multicenter, multireader, multifield-strength validation study. *Invest Radiol*. 2018;53:689–697.
24. Poot DH, Van Meir V, Sijbers J. General and efficient super-resolution method for multi-slice MRI. *Med Image Comput Comput Assist Interv*. 2010;13(Pt 1):615–622.
25. Plenge E, Poot DH, Bernsen M, et al. Super-resolution methods in MRI: can they improve the trade-off between resolution, signal-to-noise ratio, and acquisition time? *Magn Reson Med*. 2012;68:1983–1993.
26. Van Dyck P, Smekens C, Vanhevel F, et al. Super-resolution magnetic resonance imaging of the knee using 2-dimensional turbo spin echo imaging. *Invest Radiol*. 2020;55:481–493.
27. Omoumi P. The Dixon method in musculoskeletal MRI: from fat-sensitive to fat-specific imaging. *Skeletal Radiol*. 2022;51:1365–1369.
28. Gassenmaier S, Afat S, Nickel D, et al. Application of a novel iterative denoising and image enhancement technique in T1-weighted precontrast and postcontrast gradient echo imaging of the abdomen: improvement of image quality and diagnostic confidence. *Invest Radiol*. 2021;56:328–334.
29. Gassenmaier S, Herrmann J, Nickel D, et al. Image quality improvement of dynamic contrast-enhanced gradient echo magnetic resonance imaging by iterative denoising and edge enhancement. *Invest Radiol*. 2021;56:465–470.
30. Almansour H, Gassenmaier S, Nickel D, et al. Deep learning-based superresolution reconstruction for upper abdominal magnetic resonance imaging: an analysis of image quality, diagnostic confidence, and lesion conspicuity. *Invest Radiol*. 2021;56:509–516.
31. Afat S, Wessling D, Afat C, et al. Analysis of a deep learning–based superresolution algorithm tailored to partial fourier gradient echo sequences of the abdomen at 1.5 T: reduction of breath-hold time and improvement of image quality. *Invest Radiol*. 2022;57:157–162.
32. Beirinckx Q, Jeurissen B, Nicastro M, et al. Model-based super-resolution reconstruction with joint motion estimation for improved quantitative MRI parameter mapping. *Comput Med Imaging Graph*. 2022;100(May):102071.
33. Smith TB, Nayak KS. MRI artifacts and correction strategies. *Imaging Med*. 2010;2:445–457.
34. Noyes FR, Stabler CL. A system for grading articular cartilage lesions at arthroscopy. *Am J Sports Med*. 1989;17:505–513.
35. Crues JV, Mink J, Levy TL, et al. Meniscal tears of the knee: accuracy of MR imaging. *Radiology*. 1987;164:445–448.
36. Chapin R. Imaging of the postoperative meniscus. *Radiol Clin North Am*. 2018;56:953–964.
37. Park JS, Ryu KN, Yoon KH. Meniscal flounce on knee MRI: correlation with meniscal locations after positional changes. *Am J Roentgenol*. 2006;187:364–370.
38. Naraghi A, White LM. MR imaging of cruciate ligaments. *Magn Reson Imaging Clin N Am*. 2014;22:557–580.
39. Sanders TG, Miller MD. A systematic approach to magnetic resonance imaging interpretation of sports medicine injuries of the knee. *Am J Sports Med*. 2005;33:131–148.
40. Landis JR, Koch GG. The measurement of observer agreement for categorical data. *Biometrics*. 1977;33:159.
41. Lee SH, Lee YH, Suh JS. Accelerating knee MR imaging: compressed sensing in isotropic three-dimensional fast spin-echo sequence. *Magn Reson Imaging*. 2018;46:90–97.
42. Kammen BF, Padua EM, Karakas SP, et al. Clinical experience with two-point mDixon turbo spin echo as an alternative to conventional turbo spin echo for magnetic resonance imaging of the pediatric knee. *Pediatr Radiol*. 2019;49:791–800.
43. Nicastro M, Jeurissen B, Beirinckx Q, et al. To shift or to rotate? Comparison of acquisition strategies for multi-slice super-resolution magnetic resonance imaging. *Front Neurosci*. 2022;16:1044510.
44. Van Steenkiste G, Jeurissen B, Veraart J, et al. Super-resolution reconstruction of diffusion parameters from diffusion-weighted images with different slice orientations. *Magn Reson Med*. 2016;75:181–195.
45. Chaudhari AS, Grissom MJ, Fang Z, et al. Diagnostic accuracy of quantitative multicontrast 5-minute knee MRI using prospective artificial intelligence image quality enhancement. *Am J Roentgenol*. 2021;216:1614–1625.
46. Shakoor D, Kijowski R, Guermazi A, et al. Diagnosis of knee meniscal injuries by using three-dimensional MRI: a systematic review and meta-analysis of diagnostic performance. *Radiology*. 2019;290:435–445.
47. Dratsch T, Zäske C, Siedek F, et al. Reconstruction of 3D knee MRI using deep learning and compressed sensing: a validation study on healthy volunteers. *Eur Radiol Exp*. 2024;8:47.